

# Fine Tuning of the Rotational Rate of Light-Driven, Second Generation Molecular Motors by Fluorine Substitutions

Ivan Tambovtsev,<sup>\*,†</sup> Yorick L. A. Schmerwitz,<sup>†</sup> Gianluca Levi,<sup>†</sup> Darina D.  
Darmoroz,<sup>‡</sup> Pavel V. Nesterov,<sup>‡</sup> Tetiana Orlova,<sup>‡</sup> and Hannes Jónsson<sup>\*,†</sup>

<sup>†</sup>*Science Institute and Faculty of Physical Sciences, University of Iceland, 107 Reykjavík,  
Iceland*

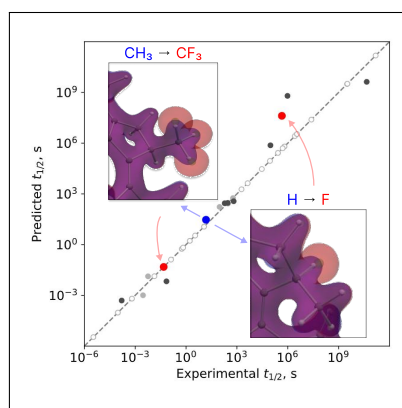
<sup>‡</sup>*Infochemistry Scientific Center, ITMO University, 9 Lomonosova street, Saint-Petersburg,  
191002, Russia*

E-mail: ivt3@hi.is; hj@hi.is

## Abstract

The relaxation time of several second generation molecular motors is analysed by calculating the minimum energy path between the metastable and stable states and evaluating the transition rate within harmonic transition state theory based on energetics obtained from density functional theory. Comparison with published experimental data shows remarkably good agreement and demonstrates the predictive capability of the theoretical approach. While previous measurements by Feringa and coworkers [Chem. Eur. J. (2017) 23, 6643] have shown that a replacement of the stereogenic hydrogen by a fluorine atom increases the relaxation time because of destabilization of the transition state for the thermal helix inversion, we find that a replacement of  $\text{CH}_3$  by a  $\text{CF}_3$  group at the same site shortens the relaxation time because of elevated energy of the metastable state without a significant shift in the transition state energy. Since these two fluorine substitutions have an opposite effect on the relaxation time, the two combined can provide a way to fine tune the rotational speed of a molecular motor.

## TOC Graphic



The development of light-powered molecular motors, where one part of a molecule rotates a full circle with respect to the rest, has been an active field of research in the past two decades and several such systems have been developed.<sup>1-3</sup> Most of these molecular motors contain a C=C double bond and one side of the bond is referred to as the ‘rotor’ while the other side is referred to as the ‘stator’. The absorption of a photon leads to a *ca.* 90° rotation of the double bond in the electronic excited state and due to steric effects further rotation results when the molecule drops back to the ground electronic state. At that point the system is in a metastable state from which a thermally induced transition to a more stable state, the so-called thermal helix inversion (THI), sets the stage again for the completion of the 360° rotational cycle when a second photon is absorbed. The absorbed energy from photons is thereby converted into repeatable and controllable molecular motion.<sup>4-7</sup>

A great deal of effort has focused on various structural modifications to tune both the wavelength of light capable of inducing the photochemical step of the rotation and the rate of the subsequent THI step.<sup>5,8</sup> This has led to the development of three generations of molecular motors. A particularly interesting and promising one is the second generation where only a single stereogenic element in the molecular structure is sufficient to ensure unidirectional rotation. There, the energy barriers for the two THI steps in the rotary cycle are similar, unlike the first generation of rotors.<sup>6,9-11</sup> Moreover, when the stator part of the second generation molecular motor is symmetric, the third and fourth step are essentially the same as the first and second steps.

This makes second generation molecular motors particularly suitable for the development of light-controllable materials where the molecular-scale rotational motion is amplified to a macroscopic level due to a cooperative effect on the environment. This has, in particular, been accomplished by doping a liquid crystal (LC) or a liquid crystalline network with molecular motors and it opens up new prospects for soft robotics and multifunctional soft actuators.<sup>12-15</sup> Moreover, since the photoisomerization of second-generation motors is accompanied by a change in molecular chirality that is amplified to the supramolecular level,

a variety of optical and photonic elements can also be developed.<sup>16,17</sup>

The rotation at the THI stage is typically the limiting factor in the rate of rotation. It determines the lifetime of the metastable photo-induced state and can cease the continuous unidirectional movement of a soft macroscopic motor when the illumination is interrupted.<sup>18</sup> Various ways of tuning the rate of the THI stage have therefore been explored, mainly by modifying the structure of the molecular skeleton. Another approach for tuning the properties of molecules that has been used in several different contexts is fluorination, that is the replacement of one or more hydrogen atom with fluorine. This has, for example, been used to adjust the half-life of the helical LC state of chiral azobenzenes with almost no effect on the photo absorption properties.<sup>19,20</sup> It has also been applied to second generation molecular motors by Feringa and coworkers<sup>21</sup> who showed that replacement of a hydrogen atom by a fluorine atom at the stereogenic center, i.e. the rotor's carbon atom next to the double bond, slows down the THI. Their analysis of experimentally measured rates as well as density functional theory (DFT) calculations of energy barriers led to the conclusion that the main effect of this fluorine substitution is an increase in the energy of the transition state due to steric effects while the relative free energy of the stable and metastable states is not significantly affected.<sup>21</sup>

In the present study, we explore another hydrogen to fluorine substitution, namely the replacement of a CH<sub>3</sub> group by a CF<sub>3</sub> group at the stereogenic center, and our calculations show this to have the opposite effect, namely an increase in the THI rate and thereby increased rotational speed. The reason for this is an increase in the energy of the metastable state while the transition state turns out not to be affected significantly. Harmonic transition state theory (HTST) is used to estimate the transition rate, *i.e.* pre-exponential factor in the Arrhenius rate expression as well as the energy barrier, with energy and atomic forces evaluated with DFT based on a hybrid functional (see Methods section). To test this approach, we compare calculated rates for a wide range of second generation molecular motors with experimentally determined rates and find remarkably good agreement. We also explore the

effect of replacing a C-H in the stator where steric hindrance occurs during the THI with an N atom.

The second-generation motors studied here are shown in figure 1. The sites are labelled by X, Y, Z, and have CH<sub>3</sub>, H, and CH, respectively, in the base molecule while the substitutions bring in CF<sub>3</sub>, F, or N. The absorption spectra of the stable and metastable states are also calculated to assess the effect these substitutions have on the photoabsorption steps in the rotational cycle.

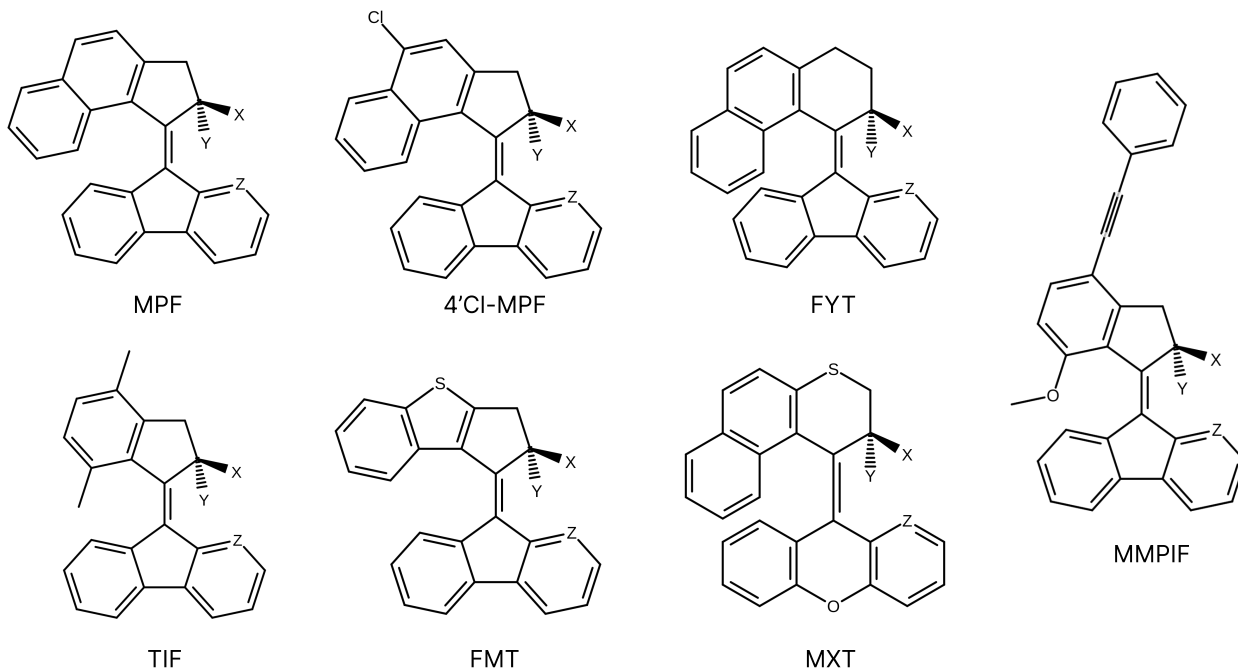


Figure 1: The molecular motors investigated in the present study to assess the effect of fluorine and nitrogen substitutions. The sites are indicated by X, Y, and Z and they have a CH<sub>3</sub>, H, and CH, respectively, in the base molecules, but CF<sub>3</sub>, F, or N in the modified molecules.

We first address the accuracy of the methodology used here to calculate the rate of relaxation from the metastable state formed after photoabsorption, *i.e.* the rate limiting THI step. Figure 2(a) compares calculated half-lives with experimentally measured values<sup>8,11,21–23,23–25</sup> for the base molecules and molecules where H has been replaced by F at site Y, as well as several other second generation molecules. The experimental data is taken from Refs.<sup>8,11,21–23,23–25</sup> (see SI). Five molecular motors with a different alkane group at site X

rather than methyl are included in the comparison since experimental data on the half-lives is available.<sup>11,23,26</sup> The close agreement between measured and calculated half-lives lends support for the theoretical methodology used here and thereby also the predictions we make for new modifications of the rotors.

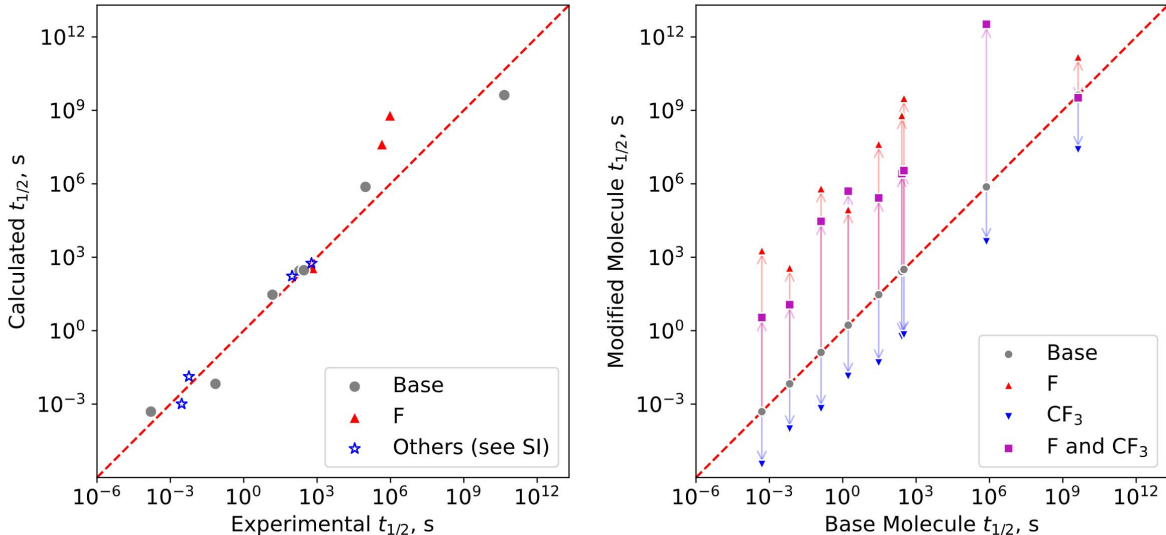


Figure 2: (a) Comparison of calculated and measured half-life of the metastable state formed after photoabsorption of several second generation molecular motors. The calculated value is obtained from the rate constant of the relaxation estimated using harmonic transition state theory and DFT evaluation of the energy and atomic forces. Data corresponding to the base molecules (shown in figure 1) is in gray, while red shows data for molecules where H has been replaced by F at site Y. Data on additional second generation motors is marked with black circles. The experimental data is obtained from Refs.<sup>8,11,21–23,23–25</sup> (see SI). The agreement between measured and calculated values is remarkably good (red dashed line indicates perfect agreement). (b) Change in calculated half-life of the metastable state by substitution of CH<sub>3</sub> by CF<sub>3</sub> at site X (blue), substitution of H by F at site Y (red), and both substitutions (purple). The F substitution increases the half-life, whereas CF<sub>3</sub> substitution decreases it. The combined effect of both substitutions in most cases gives a smaller increase in half-life compared to the F substitution alone.

Figure 2(b) shows predicted changes in the half-lives of the molecular motors by introducing CF<sub>3</sub> and F at sites X and Y. The direction and magnitude of the half-life changes induced by these substitutions are indicated by arrows. In all cases, the introduction of F at site Y increases the activation energy, while the introduction of CF<sub>3</sub> reduces it. At the same time, the pre-exponential factor typically increased by the former and reduced by the latter,

but only by a factor of 2 or so, and the change in the activation energy therefore dominates. When both substitutions are made, the half-life is in general increased, but less than for the H to F substitution alone. The combination of the two, therefore gives rise to finer tuning of the rate. The changes in pre-exponential factor and activation energy are tabulated in the SI.

As can be seen from Figure 2, the THI relaxation time varies over a wide range, nearly 15 orders of magnitude. The optimal relaxation time depends on the application and is different, for example, for liquid crystal mixtures, LC-based elastomers and polymers for a wide variety of industrial applications in optics, photonics and light-driven soft materials. Long relaxation time is suitable for data storage and information technology while short relaxation time is appropriate for switchable optical elements such as liquid crystal displays, sensors and optical gates, although if the characteristic elastic relaxation time of a chiral nematic liquid crystal significantly exceeds the photoisomer relaxation time, then the switching time is controlled by the rotational viscosity and elastic constants of the liquid crystal host. In the intermediate regime, when the LC relaxation time is comparable to the photoisomer relaxation time, programmable control of the LC orientation structure with its step-by-step reorganization can be performed.

An analysis of the effect of the two fluorine substitutions on the atomic structure of the molecules in the stable and metastable states, characterized by the two local minima, and the transition state, characterized by the first order saddle point, as well as the changes in the electronic density of the metastable state, is shown in figure 3. The structures before and after substitution are compared by lining them up along the C=C double bond. When F is introduced into site Y, the largest change in structure occurs for the transition state, while the metastable state structure is changed most when fluorine is introduced in site X. The increase in the electron density at the X and Y sites is evident when the fluorine atoms are introduced there. While it leads to increased steric hindrance in the transition state for the THI when fluorine is introduced in site Y, the main effect of introducing fluorine at site

X is evident in the structure of the metastable state.

The changes in the minimum energy paths for the THI step are also shown in figure 3. The zero of energy in each case is chosen to be the energy of the state for which the atomic structure changes the least as judged from a minimized root-mean-square deviation (RMSD). For the fluorine substitution at site Y, this is the transition structure (*i.e.* the first order saddle point) while for the substitution at site X it is the metastable state. This illustrates clearly that the main effect of the former is to raise the energy of the transition state, while the energy of the metastable state with respect to the stable state is not affected much, in agreement with the conclusions reached earlier by Feringa and coworkers 21. But, the  $\text{CH}_3$  to  $\text{CF}_3$  substitution at site X has entirely different effect, namely an increase in the energy of the metastable state while the energy of the transition structure is not changed much. As a result, the substitution at site X increases the rotational speed of the molecule, while the substitution at site Y slows it down. This is clearly illustrated for the MPF molecule in figure 3 and turns out to be the case also for the other molecules studied here (see SI).



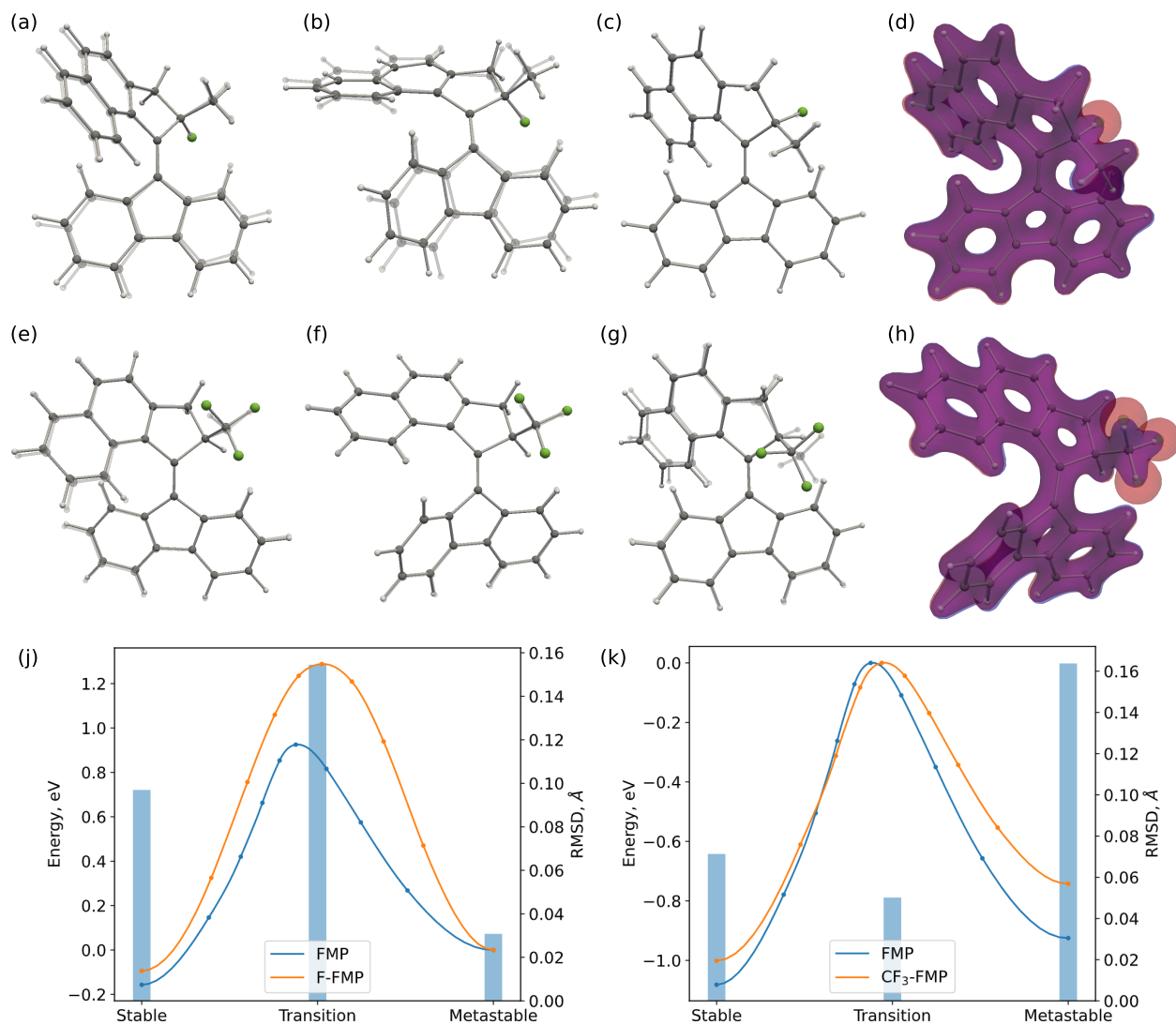


Figure 3: The effect of the H to F substitution at site Y and CH<sub>3</sub> to CF<sub>3</sub> substitution at site X of the MPF molecule (see figure 1). F atoms are green. (a,b,c) show the change in the the stable state, transition structure (*i.e.* first order saddle point), and metastable state due to the H to F substitution (F-MPF). The structures are aligned at the C=C double bond between the stator and rotor. (e,f,g) show the analogous change in structure due to the CH<sub>3</sub> to CF<sub>3</sub> substitution (CF<sub>3</sub>-MPF). (d) and (h) illustrate the change in the electron density of the metastable states, the rendered surface corresponding to density of 0.1 e/b<sup>3</sup>. (j) and (k) show the energy along the minimum energy paths for the metastable to stable state transitions of the base and modified molecules. The position of images in the converged CI-NEB calculation are indicated with points. The minimized root mean squared deviation (RMSD) between the structure of the base and modified molecules is also shown with blue bars (corresponding to axes on the right) showing how the H to F substitution mainly affects the transition structure, while the CH<sub>3</sub> to CF<sub>3</sub> substitution mainly affects the structure of the metastable state. The zero of energy for each path is chosen to be the energy of the state with the smallest RMSD, *i.e.* the metastable state of F-MPF and the transition structure of CF<sub>3</sub>-MPF. While the H to F substitution at site Y slows down the rate because the transition state energy is raised, the CH<sub>3</sub> to CF<sub>3</sub> substitution at site X increases the rate because the energy of the metastable state is increased. 9

As illustrated in fig. 3(d) for MPF, there is an increase in the electron density at site Y when the F atom is introduced. This leads to greater steric hindrance with the stator during the rotation as is evident from the changes in the transition structure and the height of the energy barrier. This can also be seen from the distance between the F atom and the H atom in the Z site of the stator in the transition structure, which is larger by more than  $0.3 \text{ \AA}$  as compared to the distance between the two H atoms in the transition structure for the base molecule (see SI).

The substitution of  $\text{CH}_3$  by  $\text{CF}_3$  at site X also increases the electron density at that site, as shown in fig. 3(h), but this turns out to introduce an increase in steric hindrance in the metastable state, as can be deduced from the atomic structure change illustrated in figure 3(e-g) and the change in energy shown in figure 3(j). The increase in distance between the H atom in the Z site of the stator and the closest F atom at site X as compared to the distance between the two corresponding H atoms in the base molecule is evident mainly in the metastable state, where it is more than  $0.5 \text{ \AA}$  while there is little increase in distance in the transition structure (see SI).

An important aspect in the design of molecular motors is the difference in wavelength of the absorption peak for the stable state and the metastable state. A larger gap corresponds to an increase in motor efficiency. Calculations of the spectra for the molecules studied here reveal that this gap increases when the  $\text{CH}_3$  to  $\text{CF}_3$  substitution site X is made at, while the gap decreases upon H to F substitution at site Y. The gap also increases when both substitutions are made.

Since the steric hindrance of the rotor with the Z site of the stator appears to be an important aspect for determining the rate of the THI, another substitution was studied where the CH at site Z is replaced by an N atom. This was tested for two of the molecules [MPF](#) and [TIF](#). Surprisingly, the main effect in both cases was an increase by *ca.*  $0.15 \text{ eV}$  increase in the energy of the metastable state, with little effect on the transition state. As a result, the half-life of the metastable state is predicted to be reduced. This substitution at

the Z site was also not found to affect the way the fluorine substitutions at sites X and Y change the rate of the THI.

In summary, the rate limiting metastable to stable state transition, *i.e.* the THI, of a variety of second-generation molecular motors has been studied theoretically using HTST and DFT. Remarkably good agreement between the calculated and published experimentally measured rates is obtained, and predictions are made for the THI rate of several new molecular motors where three types of structural modifications are made. A CH<sub>3</sub> to CF<sub>3</sub> substitution at the in stereogenic center of the rotor is found to have the opposite effect of the H to F substitution which has previously been studied by Feringa and co-workers,<sup>21</sup> namely an increase in the rate. This counterintuitive effect is explained by analysing the minimum energy path of the transition, where it is found that the CF<sub>3</sub> substitution raises the energy of the metastable state, while it has little effect on the energy of the transition state. The H to F substitution, however, raises the energy of the transition state while the metastable is barely affected, as has been concluded previously.<sup>21</sup> The third type of substitution is a CH to N substitution in the stator of the molecular motors. This substitution does not change the qualitative effects of the other substitutions on the transition rate, but it provides the possibility of bidirectionally modulating the rate. Molecules with both the F and the CF<sub>3</sub> substitution tend to have a rotation speed higher than the one of the molecules with only F substitution, but lower than that the one of the original molecule. This provides an opportunity for a fine-tuning of the rotational rate. Calculated absorption spectra indicate an enhancement of the energy efficiency of the substituted molecular motors.

## Methods

The DFT calculations make use of the B3LYP hybrid functional approximation<sup>27-29</sup> and a linear combination of atomic orbitals formalism employing the 6-31G(d,p) basis set.<sup>30,31</sup> The B3LYP functional is chosen for its proven performance in a wide range of molecular

systems, and the 6-31G(d,p) basis set is selected for its balance between computational efficiency and accuracy. The electronic structure calculations are converged to thresholds of  $10^{-8}$  a.u.,  $10^{-7}$  a.u.,  $5 \cdot 10^{-9}$  a.u., and  $5 \cdot 10^{-7}$  a.u. for the two-step energy change, the maximum component (MAX) and root mean square (RMS) of the two-step density change, and the error of the direct inversion in the iterative subspace (DIIS), respectively. The structure of the stable and metastable states of all molecular motors are optimized to a tolerance of  $10^{-4}$  a.u.,  $3 \cdot 10^{-4}$  a.u.,  $2 \cdot 10^{-3}$  a.u., and  $4 \cdot 10^{-3}$  a.u. for the RMS and MAX of the gradient and the RMS and MAX of the optimization step, respectively.

The minimum energy path for the transition from the metastable state to the stable state, i.e. the THI step, is calculated using the climbing image nudged elastic band (CI-NEB) method,<sup>32-34</sup> as implemented in the ORCA software<sup>35,36</sup> using energy weighted springs,<sup>37</sup> starting from an initial guess obtained using the sequential image depended pair potential (S-IDPP) method.<sup>7</sup> The location of the images along the path are converged to a tolerance of  $2.5 \cdot 10^{-3}$  a.u. and  $5 \cdot 10^{-3}$  a.u. in the RMS and MAX of the force perpendicular to the image tangents, respectively, with one order of magnitude tighter tolerance on the climbing image. CI-NEB is followed by a first-order saddle point search with the CI as the initial guess,<sup>37</sup> and is converged to a tolerance of  $5 \cdot 10^{-6}$  a.u.,  $3 \cdot 10^{-4}$  a.u.,  $10^{-4}$  a.u.,  $4 \cdot 10^{-3}$  a.u., and  $2 \cdot 10^{-3}$  a.u. for the two-step energy change, the MAX and RMS of the gradient, and the MAX and RMS of the optimization step, respectively.

The rate constant for the THI is calculated using the harmonic approximation to transition state theory<sup>38,39</sup>

$$k_{\text{HTST}} = \frac{\prod_i^{3N} \nu_i^{\text{min}}}{\prod_i^{3N-1} \nu_i^{\ddagger}} \exp \left[ - (E^{\ddagger} - E^{\text{min}}) / k_{\text{B}} T \right], \quad (1)$$

where  $\nu_i^{\text{min}}$  and  $\nu_i^{\ddagger}$  refer to vibrational frequency, and  $E^{\text{min}}$  and  $E^{\ddagger}$  refer to the energy of the initial state minimum and first order saddle point, respectively. The vibrational analysis is furthermore used to confirm that the stable and metastable structures are local minima

on the energy surface and the transition structures correspond to first-order saddle points. The calculated values of the pre-exponential factor, activation energy and rate constant are given in the SI. The half-life is obtained from the THI rate constant as  $\tau = \ln 2/k_{\text{HTST}}$ . The calculations are carried out for isolated molecules, while the measured half-lives are obtained from solvated molecules. Also the use of harmonic TST rather than full free energy calculations represents an approximation, as well as the inherent approximations in the DFT calculations. The remarkably close agreement between calculated and measured half-lives, illustrated in figure 2(a), is therefore a result of some cancellation of errors.

The spectra are obtained with linear-response TDDFT in the adiabatic approximation. All calculations are performed with the ORCA 5 software.<sup>35,36</sup> The data was extracted using ChemParse.

## Acknowledgement

This work was funded by the Icelandic Research Fund (grants 239970 and 217751). The calculations were carried out at the Icelandic High Performance Computing Center (IHPC).

## Supporting Information Available

The data supporting the findings of this work are available for download at Zenodo.

## References

- (1) Corra, S.; Curcio, M.; Credi, A. Photoactivated Artificial Molecular Motors. *JACS Au* **2023**, *3*, 1301–1313.
- (2) Baroncini, M.; Silvi, S.; Credi, A. Photo- and Redox-Driven Artificial Molecular Motors. *Chemical Reviews* **2020**, *120*, 200–268.

- (3) Jeong, M.; Park, J.; Kwon, S. Molecular Switches and Motors Powered by Orthogonal Stimuli. *European Journal of Organic Chemistry* **2020**, *2020*, 7254–7283.
- (4) García-López, V.; Liu, D.; Tour, J. M. Light-Activated Organic Molecular Motors and Their Applications. *Chemical Reviews* **2020**, *120*, 79–124.
- (5) Pooler, D. R. S.; Lubbe, A. S.; Crespi, S.; Feringa, B. L. Designing Light-Driven Rotary Molecular Motors. *Chemical Science* **2021**, *12*, 14964–14986.
- (6) Roke, D.; Wezenberg, S. J.; Feringa, B. L. Molecular Rotary Motors: Unidirectional Motion around Double Bonds. *Proceedings of the National Academy of Sciences of the United States of America* **2018**, *115*, 9423–9431.
- (7) Koumura, N.; Zijlstra, R. W. J.; van Delden, R. A.; Harada, N.; Feringa, B. L. Light-Driven Monodirectional Molecular Rotor. *Nature* **1999**, *401*, 152–155.
- (8) Vicario, J.; Meetsma, A.; Feringa, B. L. Controlling the Speed of Rotation in Molecular Motors. Dramatic Acceleration of the Rotary Motion by Structural Modification. *Chemical Communications* **2005**, 5910–5912.
- (9) Koumura, N.; Geertsema, E. M.; van Gelder, M. B.; Meetsma, A.; Feringa, B. L. Second Generation Light-Driven Molecular Motors. Unidirectional Rotation Controlled by a Single Stereogenic Center with Near-Perfect Photoequilibria and Acceleration of the Speed of Rotation by Structural Modification. *Journal of the American Chemical Society* **2002**, *124*, 5037–5051.
- (10) Conyard, J.; Cnossen, A.; Browne, W. R.; Feringa, B. L.; Meech, S. R. Chemically Optimizing Operational Efficiency of Molecular Rotary Motors. *Journal of the American Chemical Society* **2014**, *136*, 9692–9700.
- (11) Vicario, J.; Walko, M.; Meetsma, A.; Feringa, B. L. Fine Tuning of the Rotary Motion

- by Structural Modification in Light-Driven Unidirectional Molecular Motors. *Journal of the American Chemical Society* **2006**, *128*, 5127–5135.
- (12) Hou, J.; Long, G.; Zhao, W.; Zhou, G.; Liu, D.; Broer, D. J.; Feringa, B. L.; Chen, J. Phototriggered Complex Motion by Programmable Construction of Light-Driven Molecular Motors in Liquid Crystal Networks. *Journal of the American Chemical Society* **2022**, *144*, 6851–6860.
- (13) Lan, R.; Bao, J.; Huang, R.; Wang, Z.; Zhang, L.; Shen, C.; Wang, Q.; Yang, H. Amplifying Molecular Scale Rotary Motion: The Marriage of Overcrowded Alkene Molecular Motor with Liquid Crystals. *Advanced Materials* **2022**, *34*, 2109800.
- (14) Hou, J.; Mondal, A.; Long, G.; de Haan, L.; Zhao, W.; Zhou, G.; Liu, D.; Broer, D. J.; Chen, J.; Feringa, B. L. Photo-Responsive Helical Motion by Light-Driven Molecular Motors in a Liquid-Crystal Network. *Angewandte Chemie International Edition* **2021**, *60*, 8251–8257.
- (15) Sun, J.; Hu, W.; Zhang, L.; Lan, R.; Yang, H.; Yang, D.-K. Light-Driven Self-Oscillating Behavior of Liquid-Crystalline Networks Triggered by Dynamic Isomerization of Molecular Motors. *Advanced Functional Materials* **2021**, *31*, 2103311.
- (16) Yang, F.; Yue, B.; Zhu, L. Light-Triggered Modulation of Supramolecular Chirality. *Chemistry – A European Journal* **2023**, *29*, e202203794.
- (17) Kim, Y.; Tamaoki, N. Photoresponsive Chiral Dopants: Light-Driven Helicity Manipulation in Cholesteric Liquid Crystals for Optical and Mechanical Functions. *ChemPhotoChem* **2019**, *3*, 284–303.
- (18) Orlova, T.; Lancia, F.; Loussert, C.; Iamsaard, S.; Katsonis, N.; Brasselet, E. Revolving Supramolecular Chiral Structures Powered by Light in Nanomotor-Doped Liquid Crystals. *Nature Nanotechnology* **2018**, *13*, 304–308.

- (19) Huang, H.; Orlova, T.; Matt, B.; Katsonis, N. Long-Lived Supramolecular Helices Promoted by Fluorinated Photoswitches. *Macromolecular Rapid Communications* **2018**, *39*, 1700387.
- (20) Bléger, D.; Schwarz, J.; Brouwer, A. M.; Hecht, S. O-Fluoroazobenzenes as Readily Synthesized Photoswitches Offering Nearly Quantitative Two-Way Isomerization with Visible Light. *Journal of the American Chemical Society* **2012**, *134*, 20597–20600.
- (21) Štacko, P.; Kistemaker, J. C. M.; Feringa, B. L. Fluorine-Substituted Molecular Motors with a Quaternary Stereogenic Center. *Chemistry – A European Journal* **2017**, *23*, 6643–6653.
- (22) Pollard, M. M.; Meetsma, A.; Feringa, B. L. A Redesign of Light-Driven Rotary Molecular Motors. *Organic & Biomolecular Chemistry* **2008**, *6*, 507–512.
- (23) Pollard, M. M.; Wesenhagen, P. V.; Pijper, D.; Feringa, B. L. On the Effect of Donor and Acceptor Substituents on the Behaviour of Light-Driven Rotary Molecular Motors. *Organic & Biomolecular Chemistry* **2008**, *6*, 1605–1612.
- (24) Cnossen, A.; Pijper, D.; Kudernac, T.; Pollard, M. M.; Katsonis, N.; Feringa, B. L. A Trimer of Ultrafast Nanomotors: Synthesis, Photochemistry and Self-Assembly on Graphite. *Chemistry (Weinheim an Der Bergstrasse, Germany)* **2009**, *15*, 2768–2772.
- (25) Feringa, B. L. In Control of Motion: From Molecular Switches to Molecular Motors. *Accounts of Chemical Research* **2001**, *34*, 504–513.
- (26) Bauer, J.; Hou, L.; Kistemaker, J. C. M.; Feringa, B. L. Tuning the Rotation Rate of Light-Driven Molecular Motors. *The Journal of Organic Chemistry* **2014**, *79*, 4446–4455.
- (27) Lee, C.; Yang, W.; Parr, R. G. Development of the Colle-Salvetti Correlation-Energy



- Formula into a Functional of the Electron Density. *Physical Review B* **1988**, *37*, 785–789.
- (28) Becke, A. D. Density-Functional Exchange-Energy Approximation with Correct Asymptotic Behavior. *Physical Review A* **1988**, *38*, 3098–3100.
- (29) Becke, A. D. Density-functional Thermochemistry. III. The Role of Exact Exchange. *The Journal of Chemical Physics* **1993**, *98*, 5648–5652.
- (30) Hehre, W. J.; Ditchfield, R.; Pople, J. A. Self-Consistent Molecular Orbital Methods. XII. Further Extensions of Gaussian-Type Basis Sets for Use in Molecular Orbital Studies of Organic Molecules. *The Journal of Chemical Physics* **2003**, *56*, 2257–2261.
- (31) Weigend, F. Accurate Coulomb-fitting Basis Sets for H to Rn. *Physical Chemistry Chemical Physics* **2006**, *8*, 1057–1065.
- (32) Mills, G.; Jónsson, H.; Schenter, G. K. Reversible Work Transition State Theory: Application to Dissociative Adsorption of Hydrogen. *Surface Science* **1995**, *324*, 305–337.
- (33) Henkelman, G.; Uberuaga, B. P.; Jónsson, H. A Climbing Image Nudged Elastic Band Method for Finding Saddle Points and Minimum Energy Paths. *The Journal of Chemical Physics* **2000**, *113*, 9901–9904.
- (34) Henkelman, G.; Jónsson, H. Improved Tangent Estimate in the Nudged Elastic Band Method for Finding Minimum Energy Paths and Saddle Points. *The Journal of Chemical Physics* **2000**, *113*, 9978–9985.
- (35) Neese, F. The ORCA Program System. *WIREs Computational Molecular Science* **2012**, *2*, 73–78.
- (36) Neese, F. Software Update: The ORCA Program System—Version 5.0. *WIREs Computational Molecular Science* **2022**, *12*, e1606.

- (37) Ásgeirsson, V.; Birgisson, B. O.; Bjornsson, R.; Becker, U.; Neese, F.; Riplinger, C.; Jónsson, H. Nudged Elastic Band Method for Molecular Reactions Using Energy-Weighted Springs Combined with Eigenvector Following. *Journal of Chemical Theory and Computation* **2021**, *17*, 4929–4945.
- (38) Wigner, E. The Transition State Method. *Transactions of the Faraday Society* **1938**, *34*, 29–41.
- (39) Vineyard, G. H. Frequency Factors and Isotope Effects in Solid State Rate Processes. *Journal of Physics and Chemistry of Solids* **1957**, *3*, 121–127.

# Supporting Information for "Fine Tuning of the Rotational Rate of Light-Driven, Second Generation Molecular Motors by Fluorine Substitution"

Ivan Tambovtsev,<sup>\*,†</sup> Yorick L. A. Schmerwitz,<sup>†</sup> Gianluca Levi,<sup>†</sup> Darina D. Darmoroz,<sup>‡</sup> Pavel V. Nesterov,<sup>‡</sup> Tetiana Orlova,<sup>‡</sup> and Hannes Jónsson<sup>\*,†</sup>

<sup>†</sup>*Science Institute and Faculty of Physical Sciences, University of Iceland, 107 Reykjavík, Iceland*

<sup>‡</sup>*Infochemistry Scientific Center, ITMO University, 9 Lomonosova street, Saint-Petersburg, 191002, Russia*

E-mail: ivt3@hi.is; hj@hi.is

## Changes in atomic distances due to the fluorine substitutions

In order to analyse further the effect of the H to F substitution at site Y and  $\text{CH}_3$  to  $\text{CF}_3$  substitution at site X, the distance between the H atom in site Z on the stator and the closest atom X or Y in the MFP and F-NFP molecule was calculated for the stable state, transition structure and the metastable state. Figure 1 shows the calculated results. Clearly the main effect of the fluorine substitution at site Y is a more than  $0.3 \text{ \AA}$  increase in the transition structure while there is only a small change for the stable and metastable structures. However, the substitution at site X mainly affects the metastable structure, where the distance increases by more than  $0.5 \text{ \AA}$ .

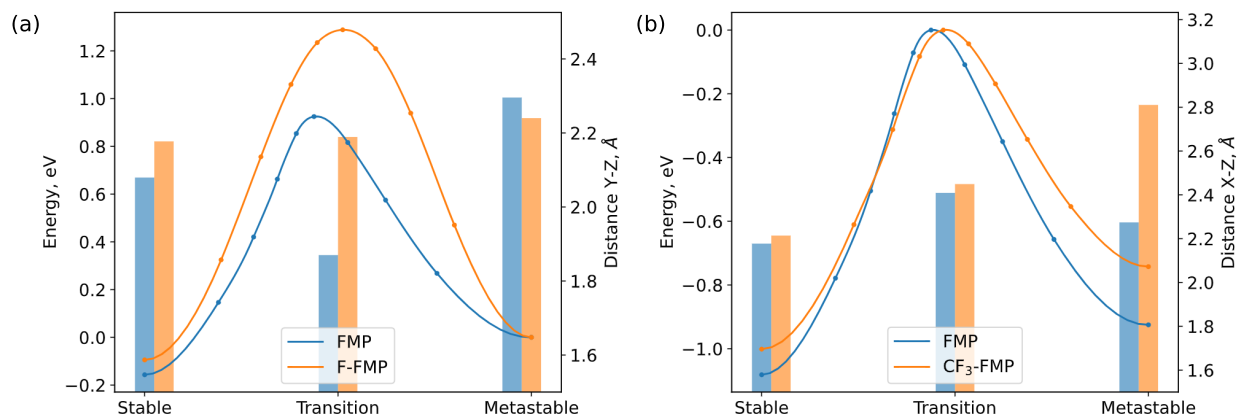


Figure 1: Shortest distances between the H atom in the Z site of the stator and the nearest atom in either the X or Y site of the rotor in the stable, transition and metastable structure of the MFP molecule and corresponding fluorinated molecule, as well as the minimum energy path shown also in figure 3 of the main text. Distance to the nearest atom at the Y site (a), and to the nearest atom in the X site (b), an H atom in MPF and an F atom in F-MPF or CF<sub>3</sub>-MPF.

## Tables

Table 1: Absorption peaks for the stable and metastable isomers of the motors

Id	$\lambda_{\text{Stable}}$ , nm	$\lambda_{\text{Metastable}}$ , nm	$\Delta\lambda$ , nm
MPF	379	410	31
F-MPF	384	414	30
CF <sub>3</sub> -MPF	378	414	36
TIF	340	367	27
CF <sub>3</sub> -TIF	340	375	35
F-TIF	343	375	31
N-MPF	376	406	30
F,N-MPF	388	401	14
CF <sub>3</sub> ,N-MPF	374	407	33
N-TIF	339	364	25
F,N-TIF	349	362	13
CF <sub>3</sub> ,N-TIF	336	371	36
FYT	360	396	36
F-FYT	370	408	38
CF <sub>3</sub> -FYT	369	415	45
MMPIF	349	375	26
F-MMPIF	351	373	22
CF <sub>3</sub> -MMPIF	345	375	30
MXT	350	414	64
F-MXT	362	443	81
CF <sub>3</sub> -MXT	343	433	90
F-FMT	349	375	27
FMT	347	365	18
CF <sub>3</sub> -FMT	350	368	18
4'Cl-MPF	388	419	32
F-4'Cl-MPF	393	422	29
CF <sub>3</sub> -4'Cl-MPF	385	424	38
CF <sub>3</sub> ,F-MPF	385	423	39
CF <sub>3</sub> ,F,N-MPF	385	415	30
CF <sub>3</sub> ,F-TIF	346	383	37
CF <sub>3</sub> ,F,N-TIF	343	378	35
CF <sub>3</sub> ,F-MMPIF	350	380	30
CF <sub>3</sub> ,F-FYT	379	431	52
CF <sub>3</sub> ,F-MXT	352	491	139
CF <sub>3</sub> ,F-FMT	353	383	31
CF <sub>3</sub> ,F-4'Cl-MPF	392	430	38

**Table 2: Full name and our abbreviation of the various compounds as well as the experimentally measured rates used for comparison with the calculated results in figure 2(a) of the main text**

Acronym	Full Name	$t_{1/2}, s$
MPF <sup>1</sup>	9-(2-Methyl-2,3-dihydro-1H-cyclopenta[a]naphthalen-1-ylidene)-9H-fluorene	$1.90 \times 10^2$
F-MPF <sup>2</sup>		$9.59 \times 10^5$
TIF <sup>3</sup>	9-(2,4,7-Trimethyl-2,3-dihydro-1H-inden-1-ylidene)-9H-fluorene	$1.50 \times 10^1$
F-TIF <sup>2</sup>		$4.49 \times 10^5$
FYT <sup>4</sup>	(3R)-4-(9H-Fluoren-9-ylidene)-3-methyl-1,2,3,4-tetrahydrophenanthrene	$4.52 \times 10^{10}$
MMPIF <sup>5</sup>		$1.60 \times 10^{-4}$
MXT <sup>6</sup>	3-Methyl-4-(9H-xanthen-9-ylidene)-3,4-dihydro-2H-1-thiaphenanthrene	$9.50 \times 10^4$
4'Cl-MPF <sup>7</sup>	9-(2-Methyl-2,3-dihydro-1H-cyclopenta[a]naphthalen-1-ylidene)-9H-fluorene	$2.88 \times 10^2$
FMT <sup>8</sup>	3-(9-Fluorenylidene)-4-methyl-7-thiatricyclo[6.4.0.02,6]dodeca-1(8),2(6),9,11-tetraene	$7.00 \times 10^{-2}$
F-FMT <sup>2</sup>		$6.42 \times 10^2$
PPF <sup>1</sup>	9-{4-Phenyltricyclo[7.4.0.02,6]trideca-1(13),2(6),7,9,11-pentaen-3-ylidene}fluorene	$5.87 \times 10^2$
IPF <sup>1</sup>	9-{4-Isopropyltricyclo[7.4.0.02,6]trideca-1(13),2(6),7,9,11-pentaen-3-ylidene} fluorene	$9.47 \times 10^1$
TPF <sup>1</sup>	9-{4-tert-Butyltricyclo[7.4.0.02,6]trideca-1(13),2(6),7,9,11-pentaen-3-ylidene} fluorene	$5.73 \times 10^{-3}$
TDIF <sup>9</sup>	9-(2-tert-Butyl-4,7-dimethyl-1-indanylidene)fluorene	$2.90 \times 10^{-3}$

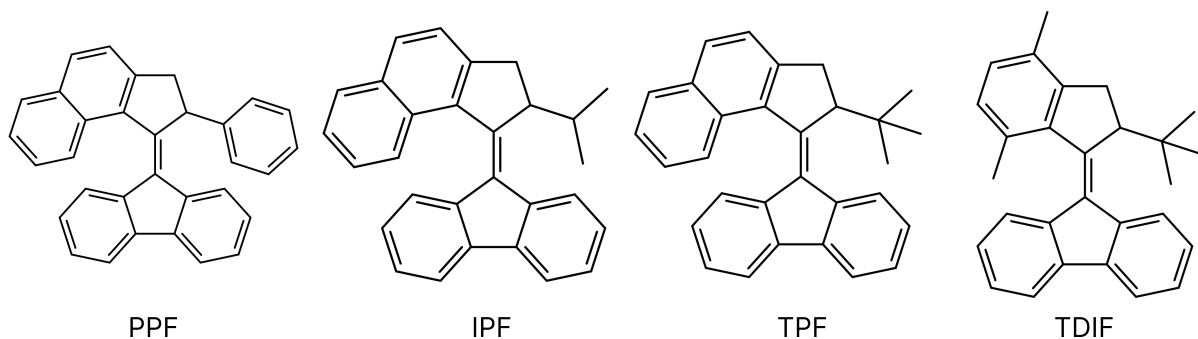


Figure 2: Second generation motors without methyl group

**Table 3: Calculated half-life as well as the corresponding pre-exponential factor (in Hz) and the energy barrier (eV) for the HTST rate constant of the THI.**

Molecule	$t_{1/2}, s$	$A, 10^{12}/s$	$\Delta E, eV$
MPF	$2.81 \times 10^2$	3.24	0.90
F-MPF	$6.25 \times 10^8$	4.78	1.29
CF <sub>3</sub> -MPF	$5.67 \times 10^{-1}$	1.75	0.72
TIF	$2.96 \times 10^1$	0.83	0.81
CF <sub>3</sub> -TIF	$4.80 \times 10^{-2}$	0.48	0.63
F-TIF	$4.15 \times 10^7$	1.33	1.18
N-MPF	$1.67 \times 10^0$	2.05	0.76
F,N-MPF	$8.93 \times 10^4$	2.20	1.04
CF <sub>3</sub> ,N-MPF	$1.35 \times 10^{-2}$	6.05	0.66
N-TIF	$1.30 \times 10^{-1}$	1.20	0.68
F,N-TIF	$6.37 \times 10^5$	0.51	1.05
CF <sub>3</sub> ,N-TIF	$6.46 \times 10^{-4}$	2.12	0.55
FYT	$4.22 \times 10^9$	2.03	1.32
F-FYT	$1.52 \times 10^{11}$	2.24	1.41
CF <sub>3</sub> -FYT	$2.47 \times 10^7$	1.36	1.17
MMPIF	$4.93 \times 10^{-4}$	0.82	0.52
F-MMPIF	$1.86 \times 10^3$	2.74	0.94
CF <sub>3</sub> -MMPIF	$3.40 \times 10^{-6}$	0.59	0.38
MXT	$7.50 \times 10^5$	4.26	1.11
F-MXT	$1.82 \times 10^{10}$	2.10	1.30
CF <sub>3</sub> -MXT	$4.29 \times 10^3$	2.93	0.97
F-FMT	$3.67 \times 10^2$	4.48	0.92
FMT	$6.76 \times 10^{-3}$	2.31	0.62
CF <sub>3</sub> -FMT	$9.54 \times 10^{-5}$	1.32	0.49
4'Cl-MPF	$2.95 \times 10^2$	2.97	0.90
F-4'Cl-MPF	$3.14 \times 10^9$	1.42	1.30
CF <sub>3</sub> -4'Cl-MPF	$6.70 \times 10^{-1}$	1.44	0.72
CF <sub>3</sub> ,F-MPF	$2.63 \times 10^6$	3.75	1.14
CF <sub>3</sub> ,F,N-MPF	$5.00 \times 10^5$	2.30	1.08
CF <sub>3</sub> ,F-TIF	$2.65 \times 10^5$	0.98	1.05
CF <sub>3</sub> ,F,N-TIF	$2.95 \times 10^4$	0.90	0.99
CF <sub>3</sub> ,F-MMPIF	$3.44 \times 10^0$	0.75	0.75
CF <sub>3</sub> ,F-FYT	$3.26 \times 10^9$	1.37	1.30
CF <sub>3</sub> ,F-MXT	$3.29 \times 10^{12}$	1.09	1.47
CF <sub>3</sub> ,F-FMT	$1.15 \times 10^1$	2.20	0.81
CF <sub>3</sub> ,F-4'Cl-MPF	$3.48 \times 10^6$	2.90	1.14
PPF	$5.67 \times 10^2$	5.43	0.93
IPF	$1.70 \times 10^2$	1.78	0.87
TPF	$1.34 \times 10^{-2}$	3.88	0.65
TDIF	$1.01 \times 10^{-3}$	1.43	0.55

**Table 4: Replacement of H by F at site Y. Units: Energy in eV, distance in Å.  $\Delta E_{A-B}$  stands for the difference in energy barriers between states A and B for base molecule and fluorinated molecule,  $\Delta d_{\alpha-\beta}A$  stands for the difference in distance between  $\alpha$  and  $\beta$  in state A for base molecule and fluorinated molecule.**

Pair	$\Delta E_{\text{Stable-TS}}$	$\Delta E_{\text{Stable-Metastable}}$	$\Delta E_{\text{Metastable-TS}}$	$d_{z-y}$ Stable	$\Delta d_{z-y}$ Stable	$d_{z-y}$ TS	$\Delta d_{z-y}$ TS	$d_{z-y}$ Metastable	$\Delta d_{z-y}$ Metastable
(MPF,F-MPF)	0.33	-0.06	0.39	2.08	0.10	1.87	0.32	2.30	-0.06
(TIF,F-TIF)	0.33	-0.05	0.38	2.11	0.09	1.87	0.35	2.38	-0.11
(FYT,F-FYT)	-0.01	-0.10	0.10	1.96	0.14	1.95	0.23	2.02	0.08
(MMPfF,F-MMPfF)	0.37	-0.05	0.42	2.07	0.09	1.90	0.07	2.20	0.00
(MXT,F-MXT)	0.05	-0.14	0.19	2.36	0.41	2.08	-0.11	1.94	-0.03
(FMT,F-FMT)	0.28	-0.02	0.30	2.07	0.09	1.94	0.32	2.14	0.04
(4'Cl-MPF,F-4'Cl-MPF)	0.33	-0.06	0.40	2.08	0.10	1.87	0.13	2.30	-0.05
(N-MPF,F,N-MPF)	0.29	0.01	0.28	2.42	0.36	2.02	0.53	2.77	0.68
(N-TIF,F,N-TIF)	0.38	0.01	0.38	2.46	0.34	2.00	0.50	3.02	0.42

**Table 5: Replacement of CH<sub>3</sub> by CF<sub>3</sub> at site X. Units: energy in eV, distance in Å.  $\Delta E_{A-B}$  stands for the difference in energy barriers between states A and B for base molecule and fluorinated molecule,  $\Delta d_{\alpha-\beta}A$  stands for the difference in distance between  $\alpha$  and  $\beta$  in state A for base molecule and fluorinated molecule.**

Pair	$\Delta E_{\text{Stable-TS}}$	$\Delta E_{\text{Stable-Metastable}}$	$\Delta E_{\text{Metastable-TS}}$	$d_{z-x}$ Stable	$\Delta d_{z-x}$ Stable	$d_{z-x}$ TS	$\Delta d_{z-x}$ TS	$d_{z-x}$ Metastable	$\Delta d_{z-x}$ Metastable
(MPF,CF <sub>3</sub> -MPF)	-0.07	0.10	-0.18	2.18	0.04	2.41	0.04	2.27	0.54
(TIF,CF <sub>3</sub> -TIF)	-0.06	0.12	-0.18	2.19	0.03	2.38	0.03	2.25	0.55
(FYT,CF <sub>3</sub> -FYT)	0.04	0.18	-0.14	2.25	0.09	4.19	0.01	2.41	0.33
(MMPfF,CF <sub>3</sub> -MMPfF)	-0.06	0.08	-0.14	2.19	0.05	2.28	0.11	2.31	0.41
(MXT,CF <sub>3</sub> -MXT)	0.12	0.27	-0.14	2.23	0.03	3.00	-0.50	2.06	0.12
(FMT,CF <sub>3</sub> -FMT)	-0.08	0.05	-0.12	2.17	0.10	2.28	0.06	2.33	0.37
(4'Cl-MPF,CF <sub>3</sub> -4'Cl-MPF)	-0.07	0.10	-0.18	2.18	0.03	2.42	0.03	2.27	0.56
(N-MPF,CF <sub>3</sub> -N-MPF)	-0.10	-0.00	-0.10	2.69	0.27	3.91	-0.12	2.35	0.60
(N-TIF,CF <sub>3</sub> -N-TIF)	-0.10	0.03	-0.12	2.72	0.26	3.88	-0.20	2.30	0.59

## References

- (1) Vicario, J.; Walko, M.; Meetsma, A.; Feringa, B. L. Fine Tuning of the Rotary Motion by Structural Modification in Light-Driven Unidirectional Molecular Motors. *Journal of the American Chemical Society* **2006**, *128*, 5127–5135.
- (2) Štacko, P.; Kistemaker, J. C. M.; Feringa, B. L. Fluorine-Substituted Molecular Motors with a Quaternary Stereogenic Center. *Chemistry – A European Journal* **2017**, *23*, 6643–6653.
- (3) Pollard, M. M.; Meetsma, A.; Feringa, B. L. A Redesign of Light-Driven Rotary Molecular Motors. *Organic & Biomolecular Chemistry* **2008**, *6*, 507–512.
- (4) Vicario, J.; Meetsma, A.; Feringa, B. L. Controlling the Speed of Rotation in Molec-



- ular Motors. Dramatic Acceleration of the Rotary Motion by Structural Modification. *Chemical Communications* **2005**, 5910–5912.
- (5) Cnossen, A.; Pijper, D.; Kudernac, T.; Pollard, M. M.; Katsonis, N.; Feringa, B. L. A Trimer of Ultrafast Nanomotors: Synthesis, Photochemistry and Self-Assembly on Graphite. *Chemistry (Weinheim an Der Bergstrasse, Germany)* **2009**, *15*, 2768–2772.
- (6) Feringa, B. L. In Control of Motion: From Molecular Switches to Molecular Motors. *Accounts of Chemical Research* **2001**, *34*, 504–513.
- (7) Pollard, M. M.; Wesenhagen, P. V.; Pijper, D.; Feringa, B. L. On the Effect of Donor and Acceptor Substituents on the Behaviour of Light-Driven Rotary Molecular Motors. *Organic & Biomolecular Chemistry* **2008**, *6*, 1605–1612.
- (8) García-López, V.; Liu, D.; Tour, J. M. Light-Activated Organic Molecular Motors and Their Applications. *Chemical Reviews* **2020**, *120*, 79–124.
- (9) Bauer, J.; Hou, L.; Kistemaker, J. C. M.; Feringa, B. L. Tuning the Rotation Rate of Light-Driven Molecular Motors. *The Journal of Organic Chemistry* **2014**, *79*, 4446–4455.